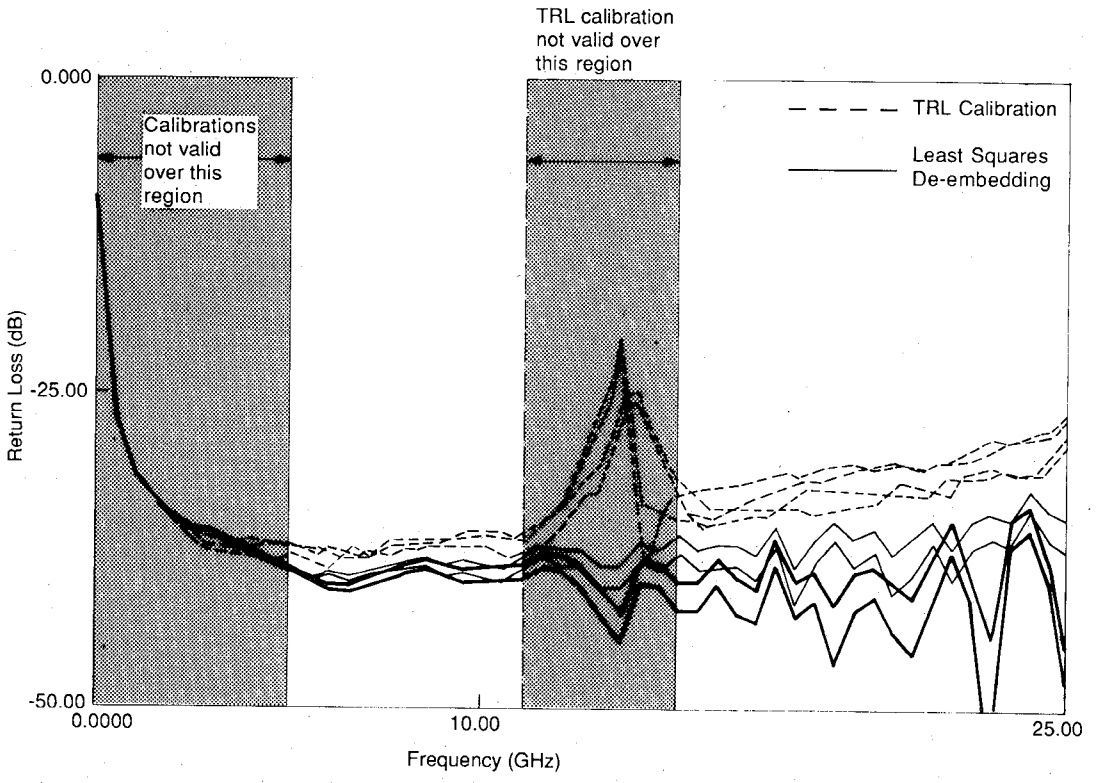

Fig. 6. The return loss of a planar load (reference [8]) de-embedded in two ways is plotted as a function of frequency. The TRL calibration is not valid over the frequencies indicated on the plot because the length of the through calibration standard approaches a half wavelength there.

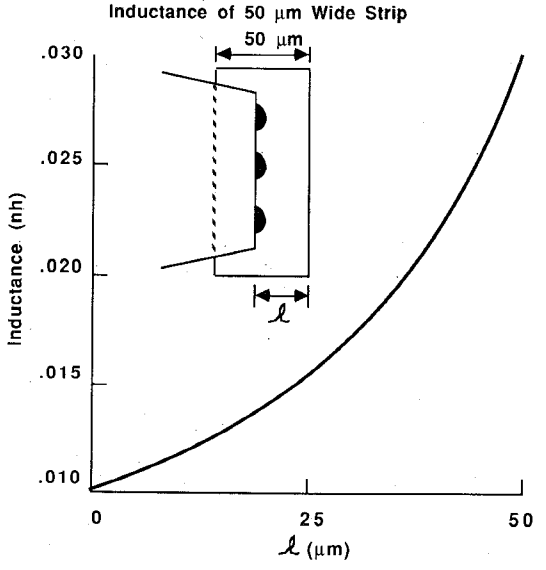

Fig. 7. The inductance of a 50-μm-wide strip as a function of probe position. The measurements were de-embedded with the least squares de-embedding procedure.

V. Conclusion

An accurate method of de-embedding coplanar probes requiring only planar CPW standards was described. This de-embedding method was shown to be suitable for making a number of microwave S parameter measurements. De-embedded measurements of commercially supplied standards independently verified their suitability for use as standards as well.

References

[1] E. W. Strid, "26 GHz wafer probing for MMIC development and manufacture," *Microwave J.*, vol. 29, p. 71, Aug. 1986.
[2] K. E. Jones, E. W. Strid, and K. R. Gleason, "Mm-wave wafer probes span 0 to 50 GHz," *Microwave J.*, vol. 30, no. 4, pp. 177–183, Apr. 1987.
[3] "Applying the HP 8510B TRL calibration for non-coaxial measurements," Hewlett Packard Product Note 8510–8, Oct. 1987.
[4] R. F. Bauer and P. Penfield, "De-embedding and unterminating," *IEEE Trans. Microwave Theory Tech.*, vol. MTT-22, pp. 282–288, Mar. 1974.
[5] The spectral domain results were obtained from the fortran program ZIMP21 supplied by Dr. T. Itoh, Dept. of Electrical Engineering, University of Texas, Austin, TX.
[6] D. F. Williams and S. E. Schwarz, "Reduction of propagation losses in coplanar waveguide," in *Proc. IEEE MTT-S Symposium*, June 1984. pp. 453–454.
[7] D. F. Williams and T. H. Miers, "A coplanar probe to microstrip transition," *IEEE Trans. Microwave Theory Tech.*, vol. MTT-36, pp. 1219–1223, July 1988.
[8] Impedance standard substrate ISS–005-16 (S.N. 12–39) supplied by Cascade Microtech, Beaverton, OR.

Millimeter-Wave Components for Use in a Variable State Four-Port Network Analyzer

JOHN V. BELLANTONI, STUDENT MEMBER, IEEE, G. CONRAD DALMAN, FELLOW, IEEE, CHARLES A. LEE, MEMBER, IEEE, AND RICHARD C. COMPTON, MEMBER, IEEE

***Abstract*—Components developed for use with a new type of network analyzer are presented. The analyzer contains a phase shifter which varies the state of the network, thus allowing accurate measurements to be made**

Manuscript received March 3, 1988; revised June 27, 1988. This work was supported by the Defense Advanced Research Projects Agency, by Alpha Industries, and by the Raytheon Company.

The authors are with the School of Electrical Engineering, Cornell University, Ithaca, NY 14853.

IEEE Log Number 8823775.

0018-9480/88/1200-1880$01.00 ©1988 IEEE

with approximately half the hardware required by conventional six-port analyzers. The phase shift is obtained using either a p-i-n diode reflection phase shifter or a mechanically positioned sliding short. Reflection measurements from two such waveguide analyzers will be presented; one operates in the 27 to 40 GHz *Ka*-band, the other in the 75 to 110 GHz *W*-band. Waveguide-to-microstrip transitions have been developed for these analyzers, to characterize millimeter-wave planar circuits. A back-to-back *Ka*-band transition was built with a maximum *VSWR* of 1.9. A second back-to-back transition displayed a maximum *VSWR* of 1.45 over the *W*-band.

I. Introduction

With a six-port network analyzer [1], phase and magnitude information can be determined using four independent power readings without the need for direct complex ratio measurements. A computer can extract magnitude and phase data from the power measurements using a set of bilinear transformations that are determined by calibration. The proliferation of low-cost personal computers makes the six-port an attractive alternative to expensive mixer systems. The six-port concept has been realized in several different configurations. In a typical six-port, four detectors are used in combination with five hybrids to provide the required independent power readings. By varying the internal state of the six-port during the measurement, four measurements can be made with a smaller number of detectors and less hardware [2]–[4].

The general principle of the variable-state four-port analyzer in waveguide is conceptualized in Fig. 1(a). Readings are taken from detectors P_1 and P_2 with and without a phase shift present, giving a total of four measurements. Operation of the analyzer, including calibration, is then analogous to that of existing six-port analyzers [2], [5]. This allows us to build on the considerable research done in this area. The calibration is performed in three stages. In the first step the power level is varied to map the RF response of the HP 11517A detector diodes. Then a sliding short and sliding load calibration is performed [2]. The calibration procedure is automated by a Macintosh II via a serial analog/digital and digital/analog convertor. A detailed description of the calibration procedure and accuracy is covered elsewhere [2]. We have designed and built two reflectometers for the *Ka*- and *W*-waveguide bands (Fig. 1(b)) using this scheme. The usefulness of these analyzers has been demonstrated in developing millimeter-wave components.

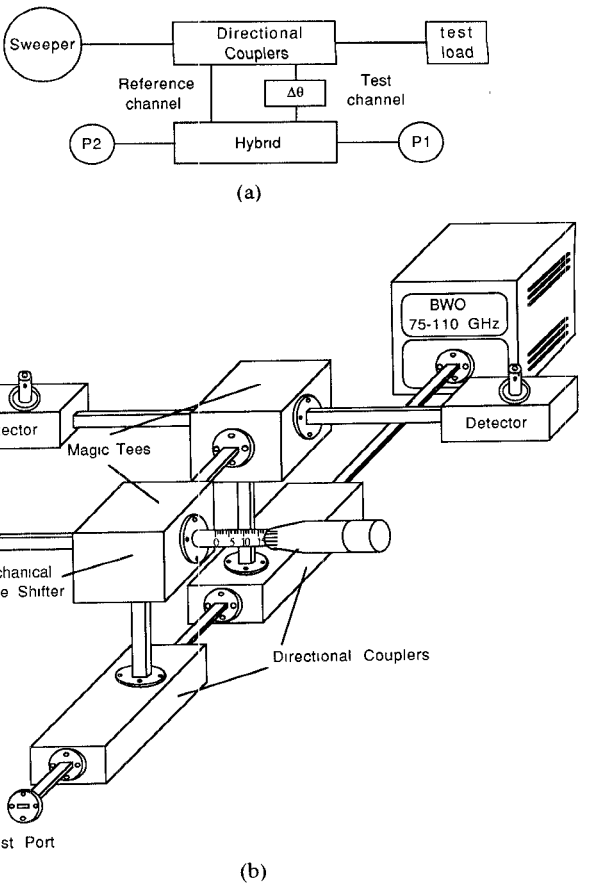

Fig. 1. (a) Conceptual diagram of the variable state four-port analyzer. (b) Perspective drawing of the variable state reflectometer for the 75 to 110 GHz band. Calibration and measurements are automated by a Macintosh II personal computer. The directional coupler in the foreground samples the reflected signal, and the coupler closest to the BWO samples the reference signal

II. Millimeter-Wave Planar Component Development

Most of the components in the RF section of the analyzer, such as the directional coupler, magic tees, and detectors, are off-the-shelf waveguide components. However, a suitable electronic phase shifter is not readily available. Also lacking are waveguide-to-microstrip adapters, essential for testing semiconductor devices.

A. Waveguide-to-Microstrip Adapter

There are several possible configurations for a waveguide-to-microstrip transition. We will describe a finline transition that gradually transforms the waveguide electric field into a quasi-TEM microstrip mode using a tapered antipodal finline. At the start of the transition, the metallization on opposite sides of the substrate is spaced apart a distance b corresponding to the height of the guide (Fig. 2). This allows for optimal coupling to the TE_{10} electric field. Along the transition the separation between the two metal layers decreases until the metal layers overlap. This has the effect of gradually rotating the field from a vertical to a horizontal alignment. The bottom finline is now the ground plane and the top metallization acts as the microstrip conductor. The tapered transition also transforms the impedance down to the desired value of 50 Ω. The finline field transition discussed here [6], [7] exhibits lower *VSWR*'s over a larger bandwidth than the more standard probe-style transitions. Finline transitions also allow easy introduction of a dc bias voltage for active devices.

Although designs for finline transitions are present in the literature, the work is often based on empirical methods with limited theoretical formulation present. In an attempt to reduce the number of iterations, a method of synthesizing finline tapers, based on nonuniform waveguide theory, was developed and applied in the design of two different kinds of finline transition. The technique outlined here draws from results distributed over a wide range of publications. The synthesis method begins with the coupled wave equations for oppositely traveling TEM waves [8]. The coupling between the waves and other relevant finline expressions are substituted into a first-order solution of the coupled wave equations. In the past, inaccurate equations for the finline cutoff f_c and impedance Z have been used [8]. Our approach uses a transverse resonance method to determine the cutoff [9] and spectral-domain results [10], [11] for the finline impedance. To get the minimum reflection in the shortest possible length of transition, without discontinuities in the finline, we use the near-optimum coupling distribution [12].

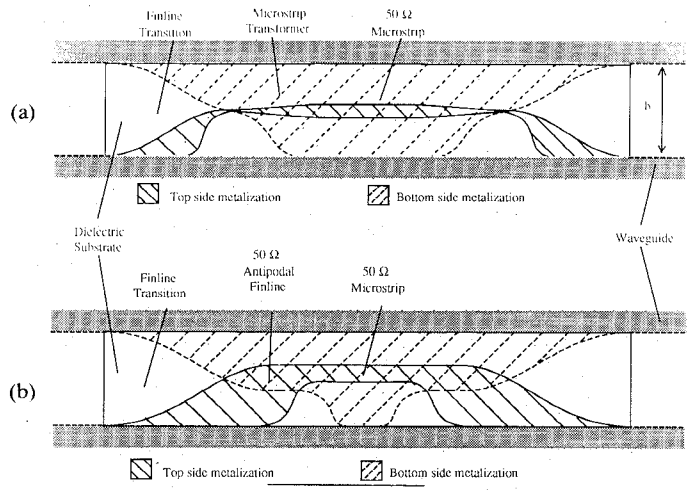

Fig. 2. Double sided circuit layout for two E-plane finline-to-microstrip transitions. The circuits were fabricated on 0.125 mm RT-Duroid 5880 substrates with dielectric constant $\epsilon_r = 2.22$. (a) 27 to 40 GHz band transition incorporating a Chebyshev transformer to match to the 50 Ω microstrip. (b) 75 to 110 GHz band transition that uses overlapped finline to match to the microstrip.

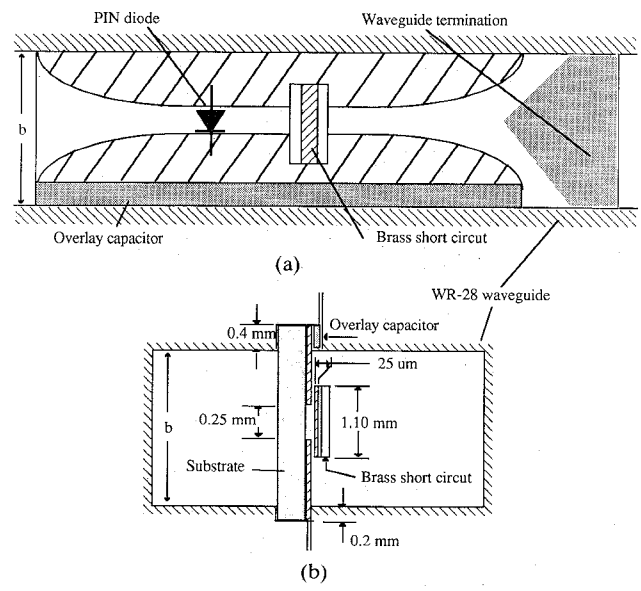

Fig. 3. (a) Circuit layout of the two-position reflection phase shifter. A signal input from waveguide on the left is reflected either at the p-i-n diode or at the short, depending on the diode bias. The substrate has a thickness of 0.25 mm and a dielectric constant $\epsilon_r = 2.22$. (b) View into the waveguide, showing the substrate mounted in an aluminum block. The finline is dc isolated from the short circuit and housing using a thin dielectric sheet that acts as a capacitor.

The coupling of a dominant wave a traveling with wavenumber $\beta(f, z)$ in the $+z$ direction to a parasitic reverse traveling wave b is modeled by the coupled equations

$$\frac{da}{dz} = -j\beta a + \kappa b$$
$$\frac{db}{dz} = \kappa a + j\beta b. \tag{1}$$

The coupling coefficient κ for a purely TEM wave is given by

$$\frac{\kappa}{2\beta_0} = \frac{1}{\sqrt{Z}} \frac{d\sqrt{Z}}{d\xi} \tag{2}$$

where

$$\xi = 2\beta_0 \left(z - \frac{L}{2} \right) \tag{3}$$

and L is the length of the transition. The quantity $-\kappa/2\beta_0$ is often defined as $CK(\xi)$ [8] where C is a normalization constant and $\beta_0 = \beta(f_0, \xi)$ is the propagation constant at some midband frequency f_0. In finline, the presence of a TE_{10} component is described by an additional term in (2) [13] so that

$$CK(\xi) \equiv -\frac{\kappa}{2\beta_0} = -\frac{1}{f_c} \frac{df_c}{d\xi} - \frac{1}{\sqrt{Z}} \frac{d\sqrt{Z}}{d\xi}. \tag{4}$$

This assumes that the TE_{10} mode propagates through a smoothly varying slot contour where there exists negligible transverse current density. Equation (4) can be rewritten as

$$CK(\xi) = -\frac{d \ln\left(f_c\sqrt{Z} \right)}{d\xi}. \tag{5}$$

Integrating (5) over ξ gives

$$\int_{-\theta}^{\xi} CK(\xi)\, d\xi = \ln \frac{f_c(\xi)\sqrt{Z(\xi)}}{f_c(-\theta)\sqrt{Z(-\theta)}}, \qquad \theta = \beta L. \tag{6}$$

Equation (6) gives the unknown finline parameters Z and f_c at any point along the line in terms of the integral of the coupling distribution up to that point of the taper.

The reflection coefficient and the coupling distribution $K(\xi)$ can be shown to be a Fourier transform pair. This allows a suitable $K(\xi)$ to be selected given a maximum reflection condition above a specified cutoff frequency. The coupling distribution $K(\xi)$ selected here is called the near-optimum distribution [12], and is the sum of two Dolph–Chebyshev functions in which the delta functions cancel out. Once the particular coupling distribution function is selected to satisfy a prescribed reflection constraint, the transition length is determined.

The method applied to solve (6) is as follows:

1) First the impedance as a function of normalized finline variables is determined from spectral-domain results given in [10] and [11]. The results are plotted and a polynomial curve is least square fitted.
2) Likewise, the cutoff frequency of the finline f_c as a function of normalized finline variables is determined from transverse resonance theory [9] and modeled as a polynomial function.
3) The integral of $K(\xi)$ is tabulated in [12]. These values are plotted as a function of normalized position and also fitted to a curve. One then has a polynomial that is a function of position on the left-hand side of (6) and the product of two polynomials that are a function of the finline dimensions on the right-hand side. A standard numerical root-finding program is used in solving these equations for the finline dimensions along the transition.

Fig. 2 illustrates two different styles of finline transition that were designed using the above synthesis procedure. The inflection in the contours is characteristic of tapers designed with even coupling distribution functions. This differs from designs that use an even function directly for the contour, such as a $\cos(z)$ dependence, without first integrating according to (6).

In Fig. 2(a) a Ka-band transition is shown. The antipodal finline taper transforms from waveguide to slightly overlapping finline. The impedance of the finline at this point is about 160 Ω,

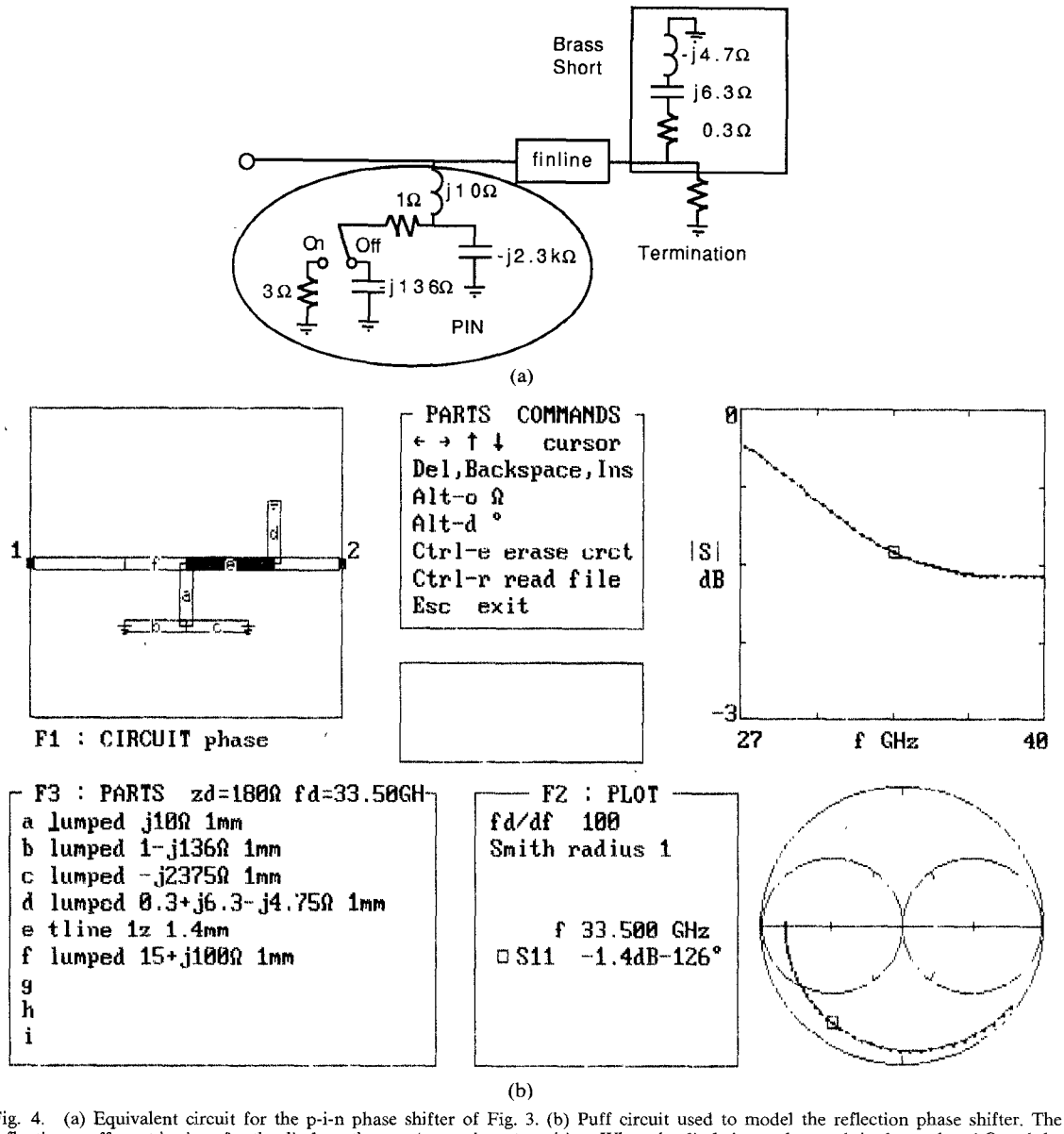

Fig. 4. (a) Equivalent circuit for the p-i-n phase shifter of Fig. 3. (b) Puff circuit used to model the reflection phase shifter. The reflection coefficient is given for the diode in the OFF (open circuit) position. When the diode is ON element b is changed to 4 Ω and the phase shifts by 90° at midband.

so a microstrip transformer is employed at that point to transform from 160 Ω to 50 Ω. The microstrip transformer is designed by integrating (2) since it is a quasi-TEM line.

In Fig. 2(b) the transition designed for the 75–110 GHz waveguide band is illustrated. The finline transforms from waveguide to antipodal finline that overlaps by approximately 20 percent of the waveguide height. At this point the impedance of the overlapping finline is 50 Ω, allowing 50 Ω microstrip to be connected directly to the finline.

B. Reflection Phase Shifter

The mechanical phase shifter shown in Fig. 1 consists of a noncontacting sliding short mounted on a magic tee. The opposite port on the magic tee is terminated and the remaining two ports serve as the input and output for the phase shifter. This type of phase shifter has very broad band performance at the expense of a 6 dB insertion loss due to the hybrid. To avoid the problems of having to reproducibly position the sliding short, and to speed up the measurement process, an electronically switchable short was developed. A two-position short was made using a p-i-n diode shunted across a tapered finline. When integrated into the 27–40 GHz analyzer, the electronic phase shifter considerably improved the performance.

The details of the *E*-plane circuitry employed in the phase shifter are shown in Fig. 3. Two discontinuities in the form of a beam lead diode and a capacitively coupled shorting septum are evenly spaced across the line to perform a high-speed switchable two-position short.

The p-i-n diode is an Alpha DSG 6470 planar beam lead device with $C_j = 35$ fF, $R_s = 4.0$ Ω, and a 150 ns minority carrier lifetime. In the OFF state the reverse-biased diode loads the line with parasitic capacitance. In the ON state, the forward bias resistance of the diode and the inductance of the beam lead limit the magnitude of the reflected signal. Effects due to the variations in C_j and R_s were studied using a computer model (Fig. 4). The particular p-i-n selected has comparatively low R_s to minimize return loss. The inherently greater C_j associated with this low R_s diode introduces additional phase shift that may be compensated by decreasing the spacing between the diode and short circuit [14]. A computer aided design program, Puff, co-

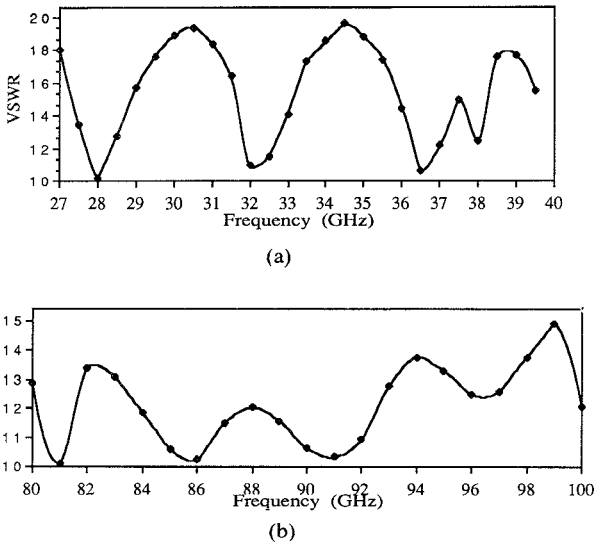

Fig. 5. Measured standing wave ratio for the two experimental transitions pictured in Fig 2. (a) 27 to 40 GHz adapter results. (b) 75–110 adapter results Both curves were measured using the computer-automated variable state four-port network analyzer.

developed by one of the authors [15], was employed in the preliminary design stages (Fig. 4). The equivalent circuit is generated in the top left screen corner from parts in the bottom left corner. The brass short circuit is represented by a lumped *RLC* circuit (element d) while the p-i-n diode is represented by three lumped impedances (elements a, b, and c). The p-i-n and short are separated by a length of transmission line (tline) with impedance $1z = 180\ \Omega$ and length 1.4 mm. The reflection coefficient for the phase shifter Γ_{11} is plotted on the magnitude plot and Smith chart on the right side of the screen. Frequency-dependent effects such as the excess electrical length of the shorting septum and finline dispersion can be stored on disk and then used by Puff to predict design trade-offs and the final performance of the phase shifter (Fig. 4).

III. Measurements

Reflection measurements of the adapters and the phase shifter were performed using two prototype variable-state reflectometers. Based on prior investigations [2], we estimate the accuracy of the measurements presented here to be better than 1 percent. In the 75 to 110 GHz setup (Fig. 1), a mechanical short is used. A p-i-n phase shifter was employed to vary the state in the 27 to 40 GHz analyzer.

The reflection coefficients of the *Ka*- and *W*-band waveguide-to-microstrip adapters were measured using a matched load to terminate one of the two waveguide ports. The results are summarized in Fig. 5. The adapters consist of three sections, a waveguide-to-microstrip transition, a length of microstrip line, and a second transition back to waveguide. A semiconductor device may be mounted on the microstrip section for testing. For the *Ka*-band adapter, each finline transition has a theoretical *VSWR* of 1.25:1, while the microstrip transformers were designed with a 1.1:1 maximum *VSWR*. Likewise, the *W*-band transition was designed to meet a total *VSWR* criterion of 1.15:1. Depending of the length of line between the two transitions, the reflections can combine constructively at some frequencies to give a total reflection equal to approximately twice the reflection from a single transition. The spacing between successive maxima in the *VSWR* plots of Fig. 5 are related to the length of microstrip line between the two transitions. Based on the design criterion, an estimated maximum *VSWR* of 2:1 is possible for the *Ka*-band adapter and a 1.7:1 *VSWR* for the *W*-band adapter. These estimates compare well with the measured data.

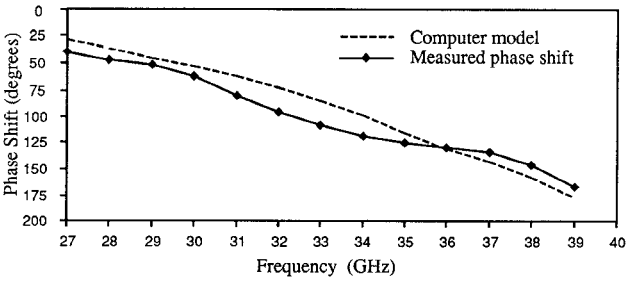

Fig. 6. Phase shift as a function of frequency for the reflection phase shifter. The computed model takes into account dispersion and frequency-dependent parasitic effects.

Fig 6 is a superposition of the measured and predicted performances for the p-i-n phase shifter in the 27 to 40 GHz waveguide band. The measurements were performed on the *Ka*-band analyzer by placing the p-i-n phase shifter at the test port. A mechanical sliding short similar to the one in the *W*-band analyzer (Fig. 1(b)) was used to provide the necessary phase shift for operating the analyzer. The computed results shown in Fig. 6 are based on the equivalent circuit of Fig. 4. Dispersion effects in the finline are included in the modeling. Not plotted in the figure is the return loss, which was better than 1.8 dB for either the ON or OFF p-i-n diode state.

IV. Conclusions

Components for use in a new type of four-port analyzer that accurately measures reflection coefficients by varying the internal state of the instrument have been presented. The analyzer is a simple, low-cost system for characterizing devices and components in the millimeter-wave region. Future work will focus on extending the analyzer to perform transmission measurements.

Acknowledgment

The authors are grateful to C. Sun for supplying the *W*-band transition that was measured. W. L. Williams provided many useful suggestions for improving the measurement accuracy.

References

[1] G. F. Engen, "The six-port reflectometer: An alternative network analyzer," *IEEE Trans. Microwave Theory Tech.*, vol. MTT-25, pp. 1075–1083, Dec. 1977.

[2] J. V. Bellantoni, G. C. Dalman, and R C. Compton, "A millimeter-wave vector network analyzer," in *Int. MTT-S Microwave Symp. Dig* (New York, NY), 1988.

[3] K. Brantervik and E. L. Kollberg, "A new four-port automatic network analyzer: Part 1—Description and performance," *IEEE Trans. Microwave Theory Tech.*, vol. MTT-33 pp. 563–568, July 1985.

[4] L. C. Oldfield, J. P. Ide, and E J Griffin, "A multistate reflectometer," *IEEE Trans. Instrum. Meas.*, vol IM-34 pp. 198–201, June 1985.

[5] G. F Engen, "Calibrating the six-port reflectometer by means of sliding terminations," *IEEE Trans Microwave Theory Tech.*, vol MTT-26 pp 951–957, Dec. 1978

[6] H. Ebner, J. Opfer, and E. C. Schweppe, "A new integrated waveguide transistor mount," in *Proc. of 13th European Microwave Conf*, Sept. 1983, pp 266–271.

[7] A K. Sharma, "A tunable waveguide-to-microstrip transition for millimeter-wave applications," in *1987 IEEE MTT-S Int Microwave Symp. Dig*, pp. 353–356.

[8] C. Schieblich, J. K Piotrowski, and J H. Hinken, "Synthesis of optimum finline tapers using dispersion formulas for arbitrary slot widths and locations," *IEEE Trans. Microwave Theory Tech.*, vol MTT-32, pp 1638–1644, Dec. 1984.

[9] J. K. Piotrowski, "Accurate and simple formulas for the dispersion in fin-lines," in *1984 IEEE MTT-S Int Microwave Symp. Dig.*, pp. 333–335

[10] L. P. Schimidt and T. Itoh, "Spectral domain analysis of dominant and higher order modes in fin-lines," *IEEE Trans. Microwave Theory Tech.*, vol. MTT-28, pp. 981–985, Sept. 1980.
[11] H. Hofmann, "Calculation of quasi-planer lines for mm-wave application," in *Proc. 1977 Int. Microwave Conf.*, pp. 381–384.
[12] R. P. Hecklen, "A near-optimum matching section without discontinuities," *IEEE Trans. Microwave Theory Tech.*, vol. MTT-20, pp. 734–739, Nov. 1972.
[13] J. H. Hinken, "Simplified analysis and synthesis of fin-line tapers," *Arch. Elek. Übertragung.*, vol. 37 pp. 375–380, Nov/Dec. 1983.
[14] P. Wahi and K. C. Gupta, "Effect of diode parameters on reflection-type phase shifters," *IEEE Trans. Microwave Theory Tech.*, vol. MTT-24, pp. 619–621, Sept. 1976.
[15] R. C. Compton and D. B. Ruthledge, *Puff: Microwave Computer Aided Design*. (Manual and Software available from authors.)

A 13 GHz YIG Film Tuned Oscillator for VSAT Applications

'YASUYUKI MIZUNUMA, YOSHIKAZU MURAKAMI, HIROYUKI NAKANO, TAKAHIRO OHGIHARA, AND TSUTOMU OKAMOTO

***Abstract*—A 13 GHz tunable oscillator using YIG film grown by LPE has been developed. A very low phase noise of −93 dBc/Hz at 10 kHz from the carrier and an output power of 11 dBm have been achieved over the entire tuning range of 500 MHz. With excellent linear tuning characteristics, this oscillator is ideal for use as a frequency-agile synthesized local oscillator in a very small aperture terminal system.**

I. Introduction

Today's *Ku*-band very small aperture terminal (VSAT) will make it possible for many more people to use commercial satellite communication services. We have utilized YIG film grown by LPE to develop a compact, low-cost, high-performance *Ku*-band tunable oscillator for use in a VSAT system [1]–[3].

As is widely recognized, local oscillator phase noise is a critical parameter in the bit error rate (*BER*) performance of a digital earth terminal [4]. From the high unloaded Q of the uniform precession mode of a YIG resonator, a very low phase noise of −93 dBc/Hz at 10 kHz from the carrier has been achieved over the entire tuning range of 500 MHz.

A compact magnetic circuit has been constructed of a permanent magnet supplying the dc magnetic field required to resonate the YIG film at 13 GHz, and a small tuning coil covering the 500 MHz tuning range. By appropriate design of the gallium substitution in the YIG film, temperature compensation between the permanent magnet and the YIG film has been achieved [1]. This approach enabled us to realize a YIG-tuned oscillator (YTO) of compact size, low power consumption for biasing field, and rapid tuning response.

Because of its low phase noise, high output power, and linear tuning characteristics, this oscillator is ideal for use as a frequency-agile synthesized local oscillator in a VSAT system. As the local oscillator selects the different channels in the up-conversion and down-conversion RF sections, it makes the construction of the earth terminal much simpler than that of a terminal using a fixed-frequency dielectric resonator local oscillator (DRO) and block conversion.

This paper will first describe the fabrication of the tunable oscillator using YIG film. The design criteria of the YIG film resonator and the output matching network to achieve low phase noise and high output power will then be discussed. The relation between phase noise, temperature, and biasing voltage V_{ds} will then be described. Finally, the tuning characteristic and the drift of the frequency and output power over the temperature range from −30°C to +60°C will be presented.

Manuscript received April 5, 1988; revised August 1, 1988.
The authors are with the Sony Corporation Research Center, 174 Fujitsukacho, Hodogaya-ku, Yokohama, 240 Japan.
IEEE Log Number 8823770.

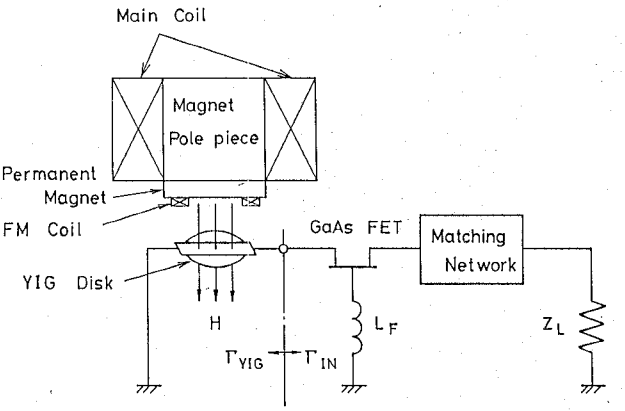

Fig. 1. Schematic structure of the complete YTO.

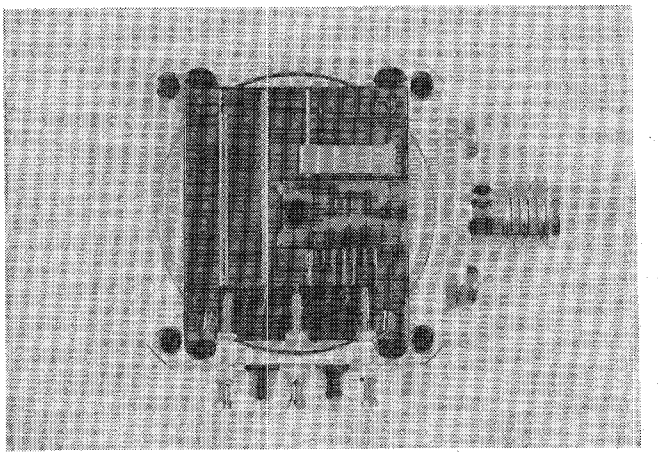

Fig. 2. Oscillator MIC.

II. Oscillator Fabrication

The schematic structure of the complete YIG film tuned oscillator and its circuit are illustrated in Figs. 1 and 2, respectively. The GaAs FET is in the common-gate configuration with the source connected to the YIG film resonator and the drain connected to the output matching circuit [5].

Fig. 3 shows the trajectory of the inverse of the input small-signal reflection coefficient Γ_{in} with frequency, and a typical reflection coefficient loop Γ_{YIG} resonating at 13 GHz. The condition for the onset of oscillation is that Γ_{in}^{-1} be encircled by Γ_{YIG}, and stable oscillation is realized when the condition $\Gamma_{in}^{-1}(A) = \Gamma_{YIG}$ is satisfied with the increase of signal level A of the GaAs FET.

0018-9480/88/1200-1885$01.00 ©1988 IEEE